Shock Compression of Liquid Deuterium up to 1 TPa

A. Fernandez-Pañella,[1] M. Millot,[1] D. E. Fratanduono,[1] M. P. Desjarlais,[2] S. Hamel,[1] M. C. Marshall,[1] D. J. Erskine,[1] P. A. Sterne,[1] S. Haan,[1] T. R. Boehly,[3] G. W. Collins,[1,3] J. H. Eggert,[1] and P. M. Celliers[1]
[1]*Lawrence Livermore National Laboratory, Livermore, California 94550, USA*
[2]*Sandia National Laboratories, Albuquerque, New Mexico 87185, USA*
[3]*Departments of Mechanical Engineering, Physics and Astronomy, and Laboratory for Laser Energetics, University of Rochester, Rochester, New York 14623, USA*

(Received 17 December 2018; revised manuscript received 11 April 2019; published 25 June 2019)

We present laser-driven shock compression experiments on cryogenic liquid deuterium to 550 GPa along the principal Hugoniot and reflected-shock data up to 1 TPa. High-precision interferometric Doppler velocimetry and impedance-matching analysis were used to determine the compression accurately enough to reveal a significant difference as compared to state-of-the-art *ab initio* calculations and thus, no single equation of state model fully matches the principal Hugoniot of deuterium over the observed pressure range. In the molecular-to-atomic transition pressure range, models based on density functional theory calculations predict the maximum compression accurately. However, beyond 250 GPa along the principal Hugoniot, first-principles models exhibit a stiffer response than the experimental data. Similarly, above 500 GPa the reflected shock data show 5%–7% higher compression than predicted by all current models.

DOI: 10.1103/PhysRevLett.122.255702

Hydrogen, the most abundant element in the Universe, is the primary constituent of solar and extra-solar giant planets. While it is the simplest element, its phase diagram at high pressure is surprisingly complex [1]. Understanding its physical properties at high pressure, density, and temperature is needed for evolutionary models of gas planets and low mass stars [2–5], and to benchmark condensed matter theory. Additionally, the quest for laboratory thermonuclear fusion requires an accurate knowledge of the equation of state and transport properties of hydrogen isotopes over a broad pressure and temperature range [6]. Specifically, as the current emphasis in the inertial confinement fusion (ICF) [7] implosions at the National Ignition Facility [8] involves stronger first shocks (100–400 GPa) [9–11] than during the National Ignition Campaign (~70 GPa) [12], there is a need to extend the benchmarking database to higher pressures than currently exist.

The hydrogen principal Hugoniot, the locus of thermodynamic states reached by single shock compression starting from the ambient-pressure cryogenic liquid state, is important because it can be determined theoretically and accessed experimentally; consequently, it has been the subject of many recent experimental investigations [13–15]. Most recent theoretical models are tested against experimental Hugoniot data, which serve as an important benchmark.

Until recently, the accuracy of shock-compression experiments (4%–8% of compressed density) was insufficient to distinguish reliably between the various theoretical models. The precision was compromised by the use of aluminum as an impedance matching standard because aluminum is opaque. Additionally, those works were limited up to ~220 GPa [14,16].

The primary advance since has been the use of a transparent reference material, α quartz, that enables precise velocity measurements at the impedance match point [17]. Additionally, the shock and release behaviors of α quartz have been calibrated with high accuracy [16,18,19]. A recent study by Knudson and Desjarlais [20] employed these advances to obtain high accuracy principal Hugoniot data in the range $50 < P < 140$ GPa for liquid deuterium compressed by magnetically accelerated flyer plates. However, in the planar shock configuration used to date, this platform is limited to pressures on the order of 200 GPa.

We report principal Hugoniot data at pressures $87 < P < 550$ GPa on cryogenic liquid deuterium, and reflected-shock data to ~1 TPa (1000 GPa) with accuracy and precision adequate to test and benchmark state-of-the-art EOS models.

The experiments were performed on the Omega Laser at the University of Rochester, a frequency-tripled Nd:glass laser ($\lambda = 351$ nm light) [21]. Temporally square pulses of 2 or 3 ns in duration with between 0.6 and 4.5 kJ energy were focused to 900 μm spots using distributed phase plates [22], producing average drive intensities between 0.4 and 4.5×10^{14} W cm^{-2}.

The planar targets for the single-shock measurements comprised a beryllium ablator (90 μm thick) and a z-cut α-quartz pusher (50 μm) [Fig. 1(a) top] with a 3-μm gold x-ray absorbing layer between them. Those were attached

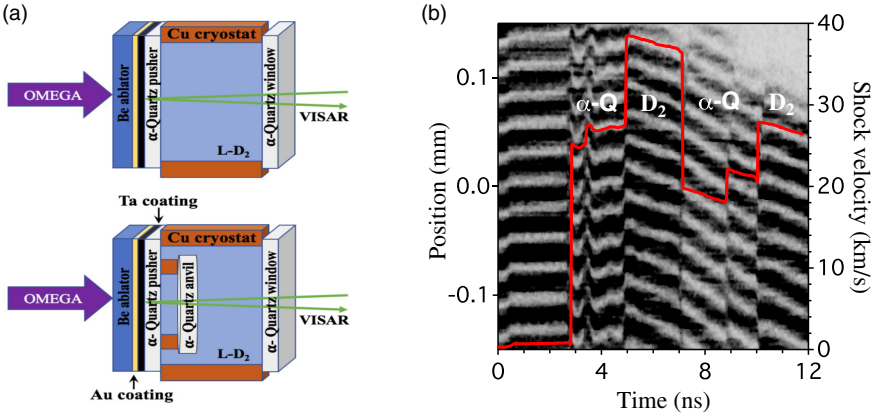

FIG. 1. (a) Schematics of a single-shock target (top) and an anvil target (bottom) design used in the experiments. The drive laser directly irradiates the target from the left while the VISAR probe beam is incident from the right side of the target. (b) Raw streak VISAR image for shot 82517 that used an anvil target, showing continuous tracking of the shock front within the α-quartz standard and the deuterium sample layers. The corresponding velocity profile (red curve) is also shown.

to a copper cryogenic cell filled with liquid deuterium ($\sim$800 μm thick) and sealed with a tilted α-quartz rear window.

The initial density of liquid deuterium was determined from the temperature of the cryogenic cell (19.0 ± 0.1 K), to be 0.173 ± 0.001 g/cm^3 and its refractive index at 532 nm, the probe wavelength, 1.138 [23]. Impedance-match measurements were obtained as the shocks traversed the α-quartz-deuterium interface. In a second set of targets [Fig. 1(a). bottom], an α-quartz anvil (50 μm) sample was immersed in the deuterium 90 μm away from the quartz pusher. This enabled single-shock measurements at the first interface (pusher-sample) and reflected-shock measurements at the second interface (sample-anvil). In a few shots, a third impedance-match measurement was obtained at the third interface (anvil-sample). The initial density of α quartz was 2.65 g/cm^3 and the refractive index along its c axis at 532 nm was 1.547 [24,25].

The drive pressures in this study were sufficient to generate optically reflective shocks [26] in both materials. *In situ* time-resolved shock velocities of the α-quartz pusher and deuterium were measured using the Velocity Interferometer System for Any Reflector (VISAR) [25–28]. The two VISARs, used to resolve the 2π phase-shift ambiguities, had $\sim$7 and $\sim$18 mm etalons to produce velocity sensitivities of 6.906 and 2.732 μm/ns/fringe in vacuum, respectively. The measured apparent velocity was then divided by the corresponding refractive index of each material at 532 nm to obtain the true velocity [26]. To minimize ghost reflections, the α-quartz surfaces facing VISAR had antireflection coatings. Two streak cameras [29] were used to detect the probe signal with either 9 or 15 ns temporal windows. The response time of the diagnostic was dominated by the delay time (τ) of the etalons -90 or 40 ps- and not the streak cameras which have $\sim$10 ps resolution [29].

The VISAR data were analyzed using a 1D fast Fourier transform (FFT) method to extract the phase and intensity of the fringes with an uncertainty of the phase about $\sim$5% of a fringe. Since the measured shock velocities in deuterium are 20–45 km/s in quartz and 26–61 km/s in deuterium, the resulting multiple fringe shifts increased the precision of the shock velocity measurements to be less than a percent (0.28%–0.75%).

An example of an anvil-target VISAR image and the corresponding shock velocity profile is shown in Fig. 1(b). Since both the α quartz and the cryogenic liquid deuterium were transparent at their initial densities, the probe beam passed through the target package and reflected off the Ta coating on the quartz. Its 30%–40% reflectivity matches those of the shock fronts in the quartz and in the deuterium, thus minimizing large excursions in the signal level in the streak records. Figure 1(b) shows the VISAR fringe shifts corresponding to the velocity of the reflecting shock propagating through the pusher (α quartz), the sample (D_2), the anvil (α quartz) and a second layer of the sample (D_2). At early times ($t < 1$ ns) we observed a weak nonionizing compression wave caused by the expansion of the Au layer (heated by keV bremsstrahlung x rays). The main shock enters the quartz at $t \approx 3$ ns, and overtakes the weak compression wave shortly afterwards ($t \approx 3.5$ ns); consequently, the weak precompression does not affect the subsequent events (at times $t > 5$ ns). The shock wave is planar over a width of at least 300 um and its strength decays as the shock front transits the α-quartz pusher and propagates throughout the rest of the target. The jumps in velocity as the shock moves into and out of the first D_2 sample layer are readily apparent at $\sim$4.9 and $\sim$7.1 ns, respectively. The velocity jump seen within the quartz anvil (at $\sim$8.8 ns) results from a reverberating shock between the anvil and pusher surfaces which catches up to the main shock before reaching out the anvil-D_2 interface. The

velocity jump at ~10 ns corresponds to the shock emerging from the quartz anvil and entering the second D_2 layer.

In each VISAR leg the shock velocities in the quartz (U_S^Q) and the deuterium (U_S^D) were extrapolated to the quartz-D_2 interface using a linear fit over 300 ps on either side of the interface. The results from the two legs were combined in a weighted average to account for different sensitivities of the two measurements.

Through impedance matching [16,30] using α quartz as the reference standard we determined the particle velocity behind the shock in the D_2 sample. Several shocks had velocities (U_S^Q) beyond the experimentally calibrated quartz EOS [16,18]. For those experiments we used the extended quartz EOS and release path by Desjarlais *et al.* using FPMD calculations [31]. See the Supplemental Material [32] for further details of the data analysis and the summary of the principal Hugoniot experimental data which is listed in Table S-I.

Ten measurements were performed over the pressure range of 87 to 550 GPa as illustrated in Fig. 2. These new data at the Omega facility have higher accuracy and are less scattered than the data collected in the same facility more than 10 years ago by Hicks *et al.*. [14], due to improvements in the equipment, methods, and calibration of the reference standard. It is noteworthy that our lowest pressure (87 GPa) state is consistent with the recent results from flyer-plate impact experiments performed at the Z facility by Knudson *et al.* [20], showing a compression of ~4.5. This agreement of results from different experimental platforms is important in studies at such extreme states. More importantly, it is in this pressure region, where the molecular-to-atomic (MA) transition is expected to occur, that theoretical models disagree most. The tabular EOS model derived by Caillabet *et al.* [35] best predicts the observed compressions at 40–100 GPa. At these conditions this model is mostly constrained by density functional theory molecular dynamics (DFT-MD) simulations performed with the Perdew-Burke-Ernzerhof (PBE) exchange-correlation functional [36]. In contrast, the "chemical" equation of state (EOS) models (Kerley [37] and SESAME 5267 [38]) underestimate the maximum compression by ~4.5% and ~8%, respectively. Interestingly, the FPEOS model by Hu *et al.*, which is also constrained by PBE-DFT-MD in this range [39], predicts a stiffer response and underestimates the maximum compression of D_2 by ~4.5%. In the pressure range ($100 < P < 200$ GPa), well into the dissociated liquid regime, the compression decreases slightly (to ~4.35), as suggested by the Caillabet *et al.* and Kerley models. The compression does not vary significantly from that value for pressures 250–550 GPa. Interestingly, Kerley predicts a marked increase in compression and ultimately agrees with the experimental data above 350 GPa. The SESAME 5267 and Caillabet *et al.* EOS models become stiffer above 200 GPa, showing worse agreement at high pressures. They estimate a compression ~4.2-fold which is beyond the 2.6% experimental uncertainty at the highest-pressure states. Finally, the FPEOS model, which in this range is derived from results produced with the path-integral Monte Carlo (PIMC) calculations, predicts a slightly stiffer behavior and is closer to the experimental results. These recent measurements indicate that no single model consistently describes all the details in the principal Hugoniot of liquid D_2 in the pressure range of 40 to 550 GPa. However, the Caillabet *et al.* model does predict the maximum compression and the pressure where it occurs. It also predicts a reduction in compression for higher pressures but overestimates that reduction.

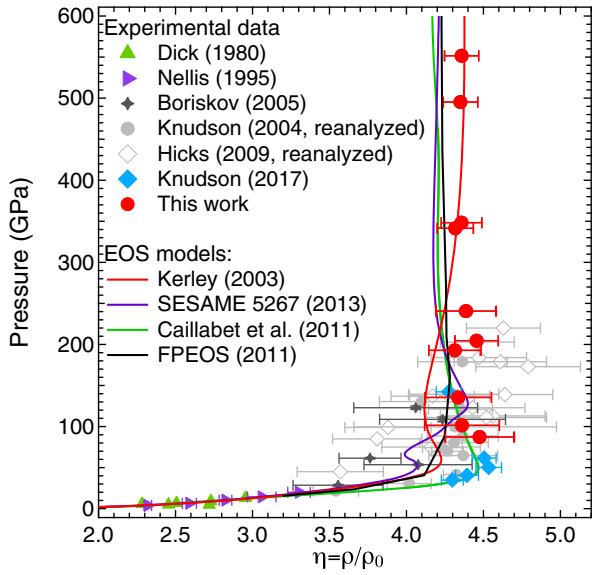

FIG. 2. Pressure vs compression for single-shock measurements of the principal Hugoniot of cryogenic liquid deuterium. Impedance-match results from explosive-driven flyer-plate impact [40] (green triangles), gas gun [41] (purple triangles), explosive-driven hemispherical shell-impact [42] (dark gray stars), magnetically driven flyer plate [13] (gray circles), laser-driven [14] (open gray diamonds), magnetically driven flyer plate [20] (blue diamonds), and laser-driven measurements (this work, red circles) are shown. The data are compared to several EOS models: Kerley [37] (solid red curve), Sesame 5267 [38] (solid purple curve), Caillabet *et al.* [35] (solid green curve), and FPEOS [39] (solid black curve).

Further insight can be obtained from the reflected-shock data. The two observables U_S^D, measured prior to reflection from the α-quartz anvil, and U_S^Q, measured immediately after reshock, are plotted in Fig. 3 along with the data from previous works and the predictions from four EOS models. In this work, four reflected-shock data points were obtained for D_2 shock velocities from 21–48 km/s. The upper plot in Fig. 3 shows the residuals of the velocity data and EOS models when normalized to the Caillabet *et al.* model. The data are summarized in Table S-VI [32]. We note that these measurements have higher accuracy and less scatter than

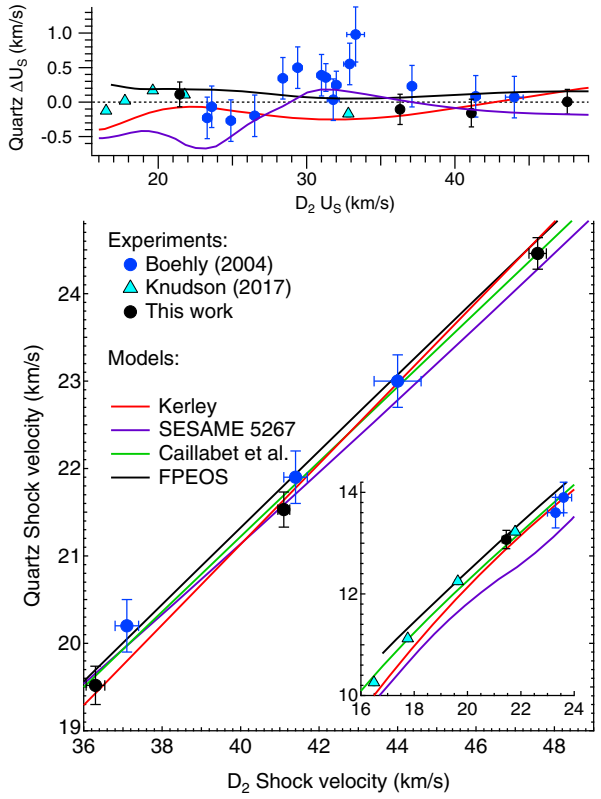

FIG. 3. Reflected-shock observables, U_S^Q vs U_S^D, from this study are shown as black filled circles. Previous laser-driven data from Ref. [43] are shown in blue filled circles and recent flyer plate measurements from Ref. [20] are shown in cyan triangles. All experimental data are plotted with error uncertainties. The colored solid lines correspond to the predictions of four EOS models. Note that the main plot covers the velocity range $36 < U_S^D < 50$ km/s while the inset covers the $16 < U_S^D < 24$ km/s. Top: Velocity residuals of the different data sets and EOS models with respect to the Caillabet *et al.* model.

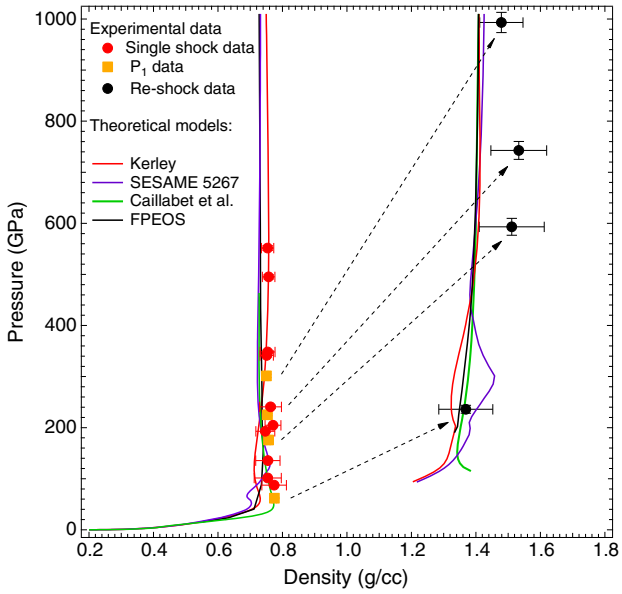

FIG. 4. Single-shock and reflected-shock compressed densities of cryogenic liquid deuterium. The orange squares correspond to (P_1, ρ_1) states, the shock state in D_2 prior to reflection from the quartz anvil (as the shock wave was not steady [32]). The red circles correspond to the single-shock data shown in Fig. 2 and the black circles correspond to the D_2 reshock states. The dashed arrows are guides to the eye and they link the single and reflected-shock states. The solid color lines correspond to four EOS models (as in Fig. 2).

previous measurements [43] and again are in good agreement with recent data from the Z facility [20]. The corresponding curves predicted by the different deuterium EOS models were calculated using the α-quartz calibration shown in Tables S-II and S-III of the Supplemental Material [32] and the impedance-matching conditions at the deuterium-quartz interface. The differences in the values of the observables (U_S^Q, U_S^D) among the EOS models and the new experimental data are overall quite small.

While the data in Fig. 3 are important for comparing among different experiments to check for systematic effects, they are not a useful test of the models: the apparent agreement with the models on the U_S^D vs U_S^Q plane result from a fortuitous error cancellation in the shock followed by the reflected shock process (see Supplemental Material [32]).

Figure 4 shows the reflected shock compression, determined by solving the Rankine-Hugoniot conditions for the reflected shock states using the known initial shock state (from the fitted Hugoniot, shown as P_1 data in Fig. 4) and the final state pressure and particle velocity, as given by the quartz calibration. The lowest pressure experiment, a reflected shock with incident shock pressure at ~62 GPa reaches ~240 GPa upon reflection from the quartz, and a density of 1.37 g/cm^3. The other three experiments ranging from 175 to 300 GPa incident pressure reach compressed densities of ~1.5 g/cm^3, about 8.5-fold compression above the cryogenic initial density.

To compare with the models, we used a fit to the measured Hugoniot to provide the initial states for the calculations [32]. The model-predicted reflected shock states were then determined by computing the second shock Hugoniot for each model and solving for the impedance match condition with the calibrated quartz Hugoniot. For the three experiments with higher initial shock pressures (>175 GPa), the second shock density was ~5% to ~8% higher than predicted by the models, while the experiment at 62 GPa is in agreement with the theoretical estimations. The three experiments starting at 175 GPa reach the density $\rho \sim 1.5$ g/cm^3 upon reshock and span a temperature range of 5 eV < kT < 9.5 eV (estimated from the Kerley model). At these conditions the fluid is fully dissociated, partially degenerate with $0.2 < T/T_F < 0.4$, where T_F is the Fermi temperature, and strongly coupled in the range $3.6 < \Gamma < 1.9$ where $\Gamma = e^2(4\pi n_i/3)^{1/3}/\mathrm{kT}$ is the electron-ion coupling parameter. The reflected shock Hugoniot curves predicted by all of the

models are largely in agreement with each other, suggesting a consensus for the predicted thermodynamic response of this dense fluid phase. Yet all models underestimate the compressibility of this dense state.

It is possible to account for the extra compression observed along the principal Hugoniot and the reshock states with an *ad hoc* density and temperature-dependent correction to the Helmholtz free energy, with corresponding changes to the internal energy, pressure, and entropy. The magnitude of these corrections are about 1.5% relative increase in internal energy along the principal Hugoniot and 3% increase along the reshock states. While small, they are comparable to the fitting uncertainty used to construct the EOS models. Thus, accuracy better than a few percent in the internal energy of the EOS models is needed in order to match our data.

We also considered processes that could affect energy conservation; for example, energy loss from radiative cooling can be ruled out because the blackbody flux from a 10 eV shock front along the principal Hugoniot ($\sigma_{SB}T^4 \approx 1$ GW/cm^2) is more than 3 orders of magnitude lower than the energy flux associated with the shock ($\rho_0 U_S^3/2 \approx 2.6$ TW/cm^2). Similarly, thermal conduction scale lengths are too small to affect the energy balance. Thus, the observed discrepancy must be attributed to the models. It may be useful to revisit finite-size-effects or the fixed-node approximation in PIMC calculations, or to examine whether collective excitation modes such as plasmons or ion acoustic waves are sufficiently well described in the models.

In summary, we have performed principal Hugoniot and reflected-shock measurements on liquid deuterium over a wide pressure range, expanding the maximum pressure along the principal Hugoniot by a factor of two, up to 550 GPa, and in the reflected shock measurements up to 1 TPa. Two current EOS models predict a stiffer response along the principal Hugoniot than the experimental data at pressures above 250 GPa, while two are in agreement; no single model fully agrees over the whole pressure range explored in this study. The reflected shock measurements indicate that all current EOS models underestimate the compressibility of deuterium in the dense strongly coupled partially degenerate fluid phase states for $500 < P < 1000$ GPa. These results provide a benchmark for future equation of state development in a regime that is directly relevant to inertial confinement fusion and planetary science.

The authors would like to thank Russel J. Wallace, Carol A. Davis, Eric Folsom, Renee Posadas Soriano, James Emig (LLNL), Julie Fooks (GA), and Mark Bonino (LLE) for their valuable contribution to the target preparation as well as Andrew Sorce and Joshua Kendrick for their help during the execution of the experiments. This work was performed under the auspices of the U.S. Department of Energy by Lawrence Livermore National Laboratory under Contract No. DE-AC52-07NA27344.

[1] J. M. McMahon, M. A. Morales, C. Pierleoni, and D. M. Ceperley, Rev. Mod. Phys. **84**, 1607 (2012).
[2] D. Saumon and G. Chabrier, Phys. Rev. A **44**, 5122 (1991).
[3] D. Saumon and G. Chabrier, Phys. Rev. A **46**, 2084 (1992).
[4] D. Saumon, G. Chabrier, and H. M. Van Horn, Astrophys. J. Suppl. Ser. **99**, 713 (1995).
[5] B. Militzer and D. M. Ceperley, Phys. Rev. Lett. **85**, 1890 (2000).
[6] J. A. Gaffney, S. X. Hu, P. Arnault, A. Becker *et al.*, High Energy Density Phys. **28**, 7 (2018).
[7] J. D. Lindl, J. Phys. Plasma **2**, 3933 (1995).
[8] J. D. Lindl, P. Amendt, R. L. Berger, S. G. Glendinning, S. H. Glenzer, S. W. Haan, R. L. Kauffman, O. L. Landen, and L. J. Suter, Phys. Plasmas **11**, 339 (2004).
[9] O. Hurricane, D. A. Callahan, D. T. Casey, P. M. Celliers *et al.*, Nature (London) **506**, 343 (2014).
[10] S. Le Pape, L. F. Berzak Hopkins, L. Divol, A. Pak *et al.*, Phys. Rev. Lett. **120**, 245003 (2018).
[11] D. T. Casey, C. A. Thomas, K. L. Baker, B. K. Spears *et al.*, Phys. Plasmas **25**, 056308 (2018).
[12] M. J. Edwards, P. K. Patel, J. D. Lindl *et al.*, Phys. Plasmas **20**, 070501 (2013).
[13] M. D. Knudson, D. L. Hanson, J. E. Bailey, C. A. Hall, J. R. Asay, and W. W. Anderson, Phys. Rev. Lett. **87**, 225501 (2001).
[14] D. G. Hicks, T. R. Boehly, P. M. Celliers, J. H. Eggert, S. J. Moon, D. D. Meyerhofer, and G. W. Collins, Phys. Rev. B **79**, 014112 (2009).
[15] P. Loubeyre, S. Brygoo, J. H. Eggert, P. M. Celliers, D. K. Spaulding, J. R. Rygg, T. R. Boehly, G. W. Collins, and R. Jeanloz, Phys. Rev. B **86**, 144115 (2012).
[16] M. D. Knudson and M. P. Desjarlais, Phys. Rev. Lett. **103**, 225501 (2009).
[17] M. Barrios, D. Hicks, T. Boehly, D. Fratanduono, J. Eggert, P. Celliers, G. Collins, and D. Meyerhofer, Phys. Plasmas **17**, 056307 (2010).
[18] M. D. Knudson and M. P. Desjarlais, Phys. Rev. B **88**, 184107 (2013).
[19] S. Brygoo, M. Millot, P. Loubeyre, A. E. Jenei, S. Hamel, T. Qi, P. M. Celliers, F. Coppari, J. H. Eggert *et al.*, J. Appl. Phys. **118**, 195901 (2015).
[20] M. D. Knudson and M. P. Desjarlais, Phys. Rev. Lett. **118**, 035501 (2017).
[21] T. R. Boehly *et al.*, Opt. Commun. **133**, 495 (1997).
[22] Y. Lin, G. N. Lawrence, and T. J. Kessler, Opt. Lett. **20**, 764 (1995).
[23] P. C. Souers, *Hydrogen Properties for Fusion Energy* (University of California Press, Berkeley, 1986).
[24] Quartz has a very low thermal expansivity. Upon cooling to <20 K, it is estimated that its density changes by only 0.5% and its refractive index by 0.1%, which are negligible for our purposes.
[25] G. Ghosh, Opt. Commun. **163**, 95 (1999); L. M. Barker and R. E. Hollenbach, J. Appl. Phys. **43**, 4669 (1972).
[26] P. M. Celliers, D. K. Bradley, G. W. Collins, D. G. Hicks, T. R. Boehly, and W. J. Armstrong, Rev. Sci. Instrum. **75**, 4916 (2004).
[27] L. M. Barker and K. W. Schuler, J. Appl. Phys. **45**, 3692 (1974).

[28] P. M. Celliers, G. W. Collins, L. B. Da Silva, D. M. Gold, and R. Cauble, Appl. Phys. Lett. **73**, 1320 (1998).
[29] P. A. Jaanimagi, R. Boni, D. Butler, S. Ghosh, W. R. Donaldson, and R. L. Keck, *Proc. SPIE 5580, 26th International Congress on High-Speed Photography and Photonics* (2005).
[30] P. M. Celliers, G. W. Collins, D. G. Hicks, and J. H. Eggert, J. Appl. Phys. **98**, 113529 (2005).
[31] M. P. Desjarlais, M. D. Knudson, and K. R. Cochrane, J. Appl. Phys. **122**, 035903 (2017).
[32] See Supplemental Material at http://link.aps.org/supplemental/10.1103/PhysRevLett.122.255702 for more details regarding the experimental data and analysis, which includes Refs. [33,34].
[33] Y. B. Zel'dovich and Y. P. Raizer, *Physics of Shock Waves and High-Temperature Hydrodynamic Phenomena*, edited by W. D. H. a. R. F. Probstein (Dover, Mineola, N.Y., 2002), Vol. 1.
[34] M. D. Knudson, M. P. Desjarlais, R. W. Lemke, and T. R. Mattson, M. French, N. Nettelmann, and R. Redmer, Phys. Rev. Lett. **108**, 091102 (2012).
[35] L. Caillabet, S. Mazevet, and P. Loubeyre, Phys. Rev. B **83**, 094101 (2011).
[36] J. P. Perdew, K. Burke, and M. Ernzerhof, Phys. Rev. Lett. **77**, 3865 (1996).
[37] G. I. Kerley, Equations of state for hydrogen and deuterium, Sandia National Laboratories Technical Report No. SAND2003-3613, 2003, http://dx.doi.org/10.2172/917468.
[38] D. Saumon, The sesame 5267 equation of state of deuterium, Technical Report No. LA-UR-13-20032, Los Alamos National Laboratory, 2013.
[39] S. X. Hu, B. Militzer, V. N. Goncharov, and S. Skupsky, Phys. Rev. B **84**, 224109 (2011).
[40] R. D. Dick and G. I. Kerley, J. Chem. Phys. **73**, 5264 (1980).
[41] W. J. Nellis, A. C. Mitchell, M. van Thiel, and R. J. Trainor, J. Chem. Phys. **79**, 1480 (1983).
[42] G. V. Boriskov, A. I. Bykov, R. Il'kaev, V. D. Selemir, G. V. Simakov, R. F. Trunin, V. D. Urlin, A. N. Shikin, and W. J. Nellis, Phys. Rev. B **71**, 092104 (2005).
[43] T. R. Boehly, D. G. Hicks, P. M. Celliers, T. J. B. Collins, R. Earley, J. H. Eggert, D. Jacobs-Perkins, S. J. Moon, E. Vianello, D. D. Meyerhofer, and G. W. Collins, Phys. Plasmas **11**, L49 (2004).